



Shahid Chamran
University of Ahvaz

Journal of Applied and Computational Mechanics



Research Paper

Elastic Limit Angular Velocity and Acceleration Investigation in Non-Uniform Rotating Disk under Time-Dependent Mechanical Loading

Sanaz Jafari[✉]

Department of Mechanical Engineering, Faculty of engineering, University of Bojnord, Bojnord, P. O. Box 94531-55111, Iran

Received March 11 2020; Revised May 10 2020; Accepted for publication May 10 2020.

Corresponding author: S. Jafari (s.jafari@ub.ac.ir)

© 2022 Published by Shahid Chamran University of Ahvaz

Abstract. An analytical effort is made to achieve cognition on the effect of time-dependent mechanical loading on the stress fields of rotating disks with non-uniform thickness and density. At high variable angular velocities and accelerations, evaluation of the effect of shear stress on the values of von Mises stress is significant and it is excellent to consider shear stress in this equivalent stress calculation alongside the radial and tangential stress. In the proposed analytical model, the Homotopy perturbation method (HPM) solves the general structure of rotating disks equilibrium equations in both radial and tangential directions. HPM is an efficient tool to solve linear and nonlinear equations, providing solutions in quick converging series. The results obtained through this process are then confirmed using the finite difference method and the exact solution in the literature. The effect of parameters in angular velocity and acceleration functions with the parameter in the thickness function and the effect of boundary conditions on the values of elastic limit angular velocity and acceleration are established by performing numerical examples. Furthermore, the effect of shear stress on the maximum values of von Mises stress is discussed. It is shown that shear stress has more influence on the distribution of equivalent von Mises stress in the elastic region. It is shown the introduced analytical model is useful for evaluating rotating disk with any arbitrary shape of thickness and density function, without using the commercial finite element simulation software.

Keywords: Non-uniform thickness and density disk, Homotopy perturbation method, Time-dependent loading, Shear stress, Elastic limit angular velocity and acceleration.

1. Introduction

In various engineering machines and systems such as gas turbine engines, gears, flywheel systems, turbo pumps, and turbo generator a rotating disk is an essential structural component [1-4]. Throughout normal work, the angular velocity of a rotating disk is usually constant. But, the angular velocity is changed overtime during the start or the stop process of the machine and the disk may have an angular acceleration. Hence, the stress distribution of rotating disks becomes an essential consideration of the design process in such situations. The study of real engineering problems generally includes the solution of nonlinear differential equations. It is not possible to solve these differential equations simply and usually attempts to find their exact solution fails. Most of the research in rotating disk fields is focused on the finite element simulations and numerical solutions of rotating disks with uniform and particularly variable thickness and density under constant angular velocity [1-20]. As previous research shows, numerical methods in solving nonlinear problems are not highly accurate and sometimes have high error rates. Finite element solutions also need commercial software and are costly. Based on the need for high precision solutions, no research work has been provided on analyzing mechanical behavior in a rotating disk under time-dependent mechanical loading with analytical methods to the author's knowledge. The Homotopy perturbation method (HPM) is used for the first time in this paper to obtain displacement-stress distributions in both radial and tangential direction of the rotating disk under variable mechanical loading condition. In most cases [21-25], the HPM yields a very quick convergence of the solution series. It is showing that the elastic limit angular velocity and acceleration how changes over time for different thickness and density parameters and boundary conditions.

One of the first researchers to work on the theoretical treatment of elastic-plastic rotating disks is Gamer [1], and after him, researchers continue in various aspects to these days [1-20]. Gamer provided the exact solution for the elastic-plastic reaction of a rotating solid disk with uniform thickness. Following on Gamer works; Guven investigated the fully plastic state of the solid disk with variable thickness [2-4]. Eraslan performed computational studies on the elastic-plastic mechanical behavior of annular disks with various thickness profiles, including hyperbolic, exponential and power types under different boundary conditions [5-9]. Hojjat et al. also have performed several works on rotating disks [10-15]. They studied the elastic behavior of rotating disks by variational iteration method [10], variable material property method [11], Adomian's decomposition [12] and homotopy perturbation methods [12]. The thickness and density function are considered non-uniform in these researches and parametric studies for different values of thickness and density parameters are carried out after the verification process [10-12]. They



proposed a plastic study of rotating disks by assuming a linear strain hardening model for material behavior in the plastic region by HPM [13] and variable material property method [12]. In all of these researches, constant mechanical loading is imposed on rotating disks. Hojjati et al. suggested the use of variable material properties, Runge-Kutta's and finite element methods for functionally graded rotating disks subjected to thermo-mechanical loadings [14]. In the field of optimization, Jafari et al. introduced classical and modern optimization methods in minimal weight configuration of an elastic rotating disk with variable thickness and density. They used Karush-Kuhn-Tucker, simulated annealing (SA) and particle swarm methods (PSO) and found that the performance of PSO and SA methods is simpler and provides greater flexibility [15].

Among the latest research, Alashti et al. studied the plastic behavior of a rotating disk with non-uniform thickness under a constant angular velocity by taking into consideration the models of ductile damage in simulations [16]. Zheng et al. provided stress analysis for non-uniform thickness and variable angular velocity in functionally graded rotating disks using the finite difference method [17]. Newly, Salehian et al perform thermo-elastic analysis of a functionally graded rotating hollow circular disk with variable thickness and angular velocity using the Galerkin method [18]. Shlyannikov et al. emphasis on the crack growth rate for rotating disk in gas turbine engine compressor based on the nonlinear fracture mechanics [19]. Nayak et al. used a variational iteration method to evaluate the elastic-plastic behavior of thermo-mechanically loaded FGM disks [20]. Bayat et al. solved a thermo-elastic contact problem of functionally graded materials rotating brake disk under temperature dependent material properties by Finite Element Method. The results for temperature-dependent and temperature-independent material properties are investigated and presented [21].

As a result of this introduction, it can say that the presumption in a large number of studies is that the angular velocity as mechanical loading is constant. Because of the importance of variable angular velocities on the one hand and the accuracy precision of analytical solution on the other hand, displacement-stress distributions in radial and tangential direction and the values of elastic limit angular velocity and acceleration are studied using the presented analytical model for boundary condition that occurs in real work environments. The rotating disk undergoes the time-dependent mechanical loading and governing equilibrium equations are solved by HPM. The results are compared to the exact solution for uniform disk and the results of a non-uniform disk are confirmed using the finite difference method. The material is supposed to obey an elastic-linear hardening behavior with von Mises yield criterion. The values of equivalent von Mises stress as a criterion for estimating the elastic limit of angular velocity and acceleration are implemented. Finally, a parametric analysis is performed in the form of examples for various sets of thickness parameters, boundary conditions and constants in angular velocity and acceleration functions. The material of the disk is considered as an Inconel-718 alloy in which density varied alongside the disk radius according to a special function. As illustrated in Fig. 1, the disk is assumed to be different boundary conditions. Also, a schematic configuration of equipment including the rotating disk is shown in this figure.

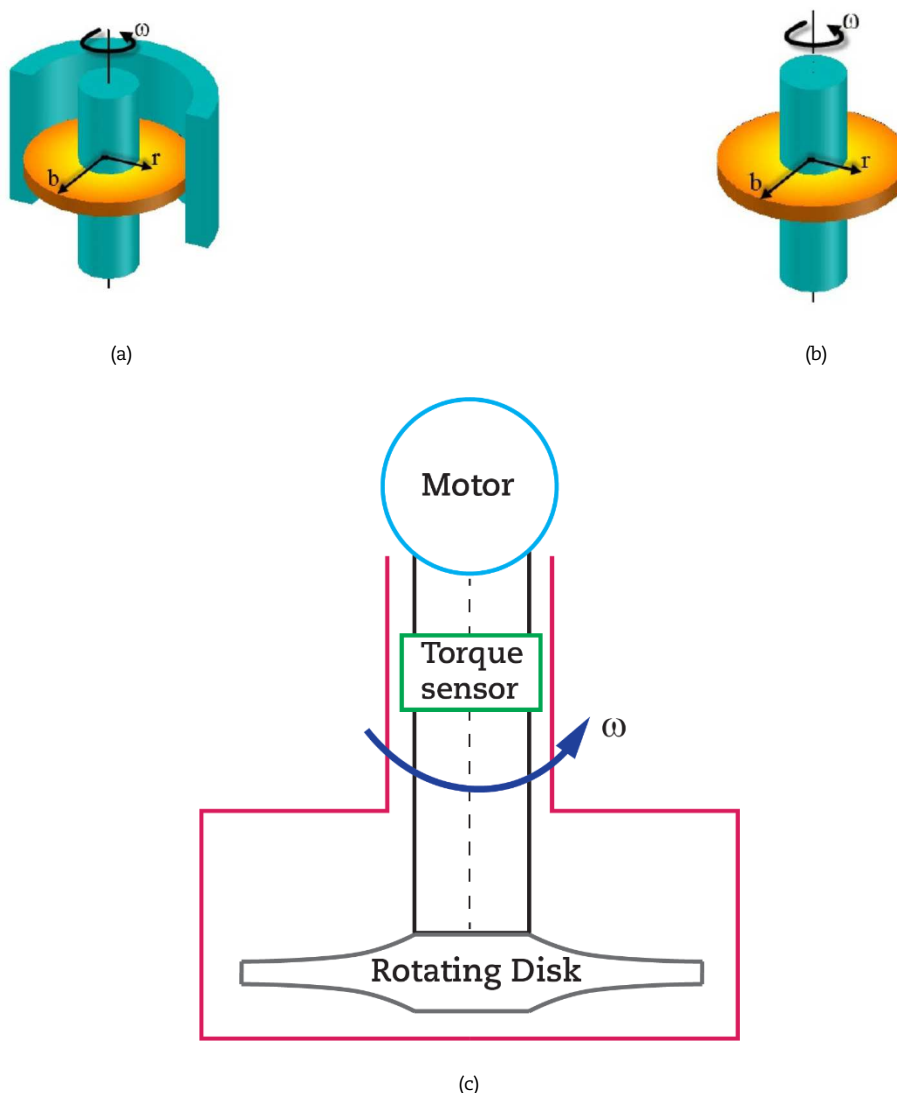


Fig. 1. a) Radially restricted-directed b) radially restricted-free c) a schematic configuration of equipment including the rotating disk



2. Disk Thickness Profile and Material Properties

The disk is symmetrical to the mid-plane and its profile is supposed to vary as a function of radius (r) as shown in Fig. 2 [12]:

$$h(r) = h_0 \left(\frac{r}{r_e} \right)^{-n} \quad (1)$$

where n is geometric parameter, r_e is the outer radius of the disk and h_0 is the thickness of the disk at $r = r_e$. The disk material is chosen as Inconel-718 having densities that change according to Eq. (2) [17]:

$$\rho(r) = \rho_0 + \rho_1 r + \rho_2 r^2 + \rho_3 r^3, \quad \rho_0 = 7800 \frac{\text{kg}}{\text{m}^3}, \quad \rho_1 = 10 \frac{\text{kg}}{\text{m}^4}, \quad \rho_2 = 100 \frac{\text{kg}}{\text{m}^5}, \quad \rho_3 = 1000 \frac{\text{kg}}{\text{m}^6} \quad (2)$$

The density function along the disk radius is shown in Fig. (2). Uniform thickness and density disk are simply obtained by setting $n = 0$ in Eq. (1) and $r = 0$ in Eq. (2), respectively. An elastic-linear hardening [2] model is used in this work to model the stress-strain relationship of the disk material:

$$\begin{cases} \varepsilon = \frac{\sigma}{E} & \sigma \leq \sigma_o \\ \varepsilon = \frac{\sigma_o}{E} + \frac{1}{E_t}(\sigma - \sigma_o) & \sigma > \sigma_o \end{cases} \quad (3)$$

where σ_o and E_t are the material yield strength and tangent modulus, respectively. Table 1 demonstrates the geometry and material properties used for the disks studied in this research.

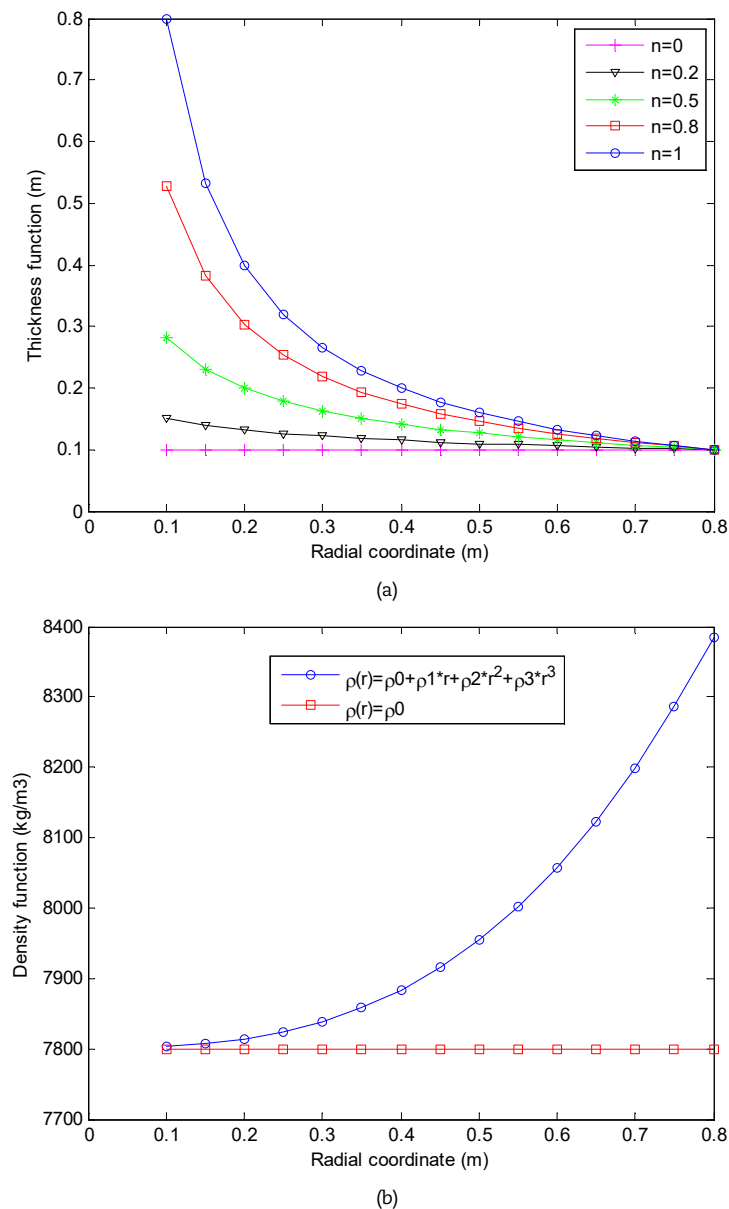


Fig. 2. a) Disk profile for different thickness parameter b) Density function



Table 1. Geometry and material properties and angular velocity constant of rotating disks [18]

Outer radius r_o (m)	Inner radius r_i (m)	Thickness at $r = r_e$	Young's modulus E (GPa)	Poisson's ratio ν	Shear modulus G (GPa)	Tangent modulus E_t (GPa)	Yield strength σ_o (MPa)	Angular velocity constant ω_o (rad/s)	Angular velocity constant λ (1/s)
0.8	0.1	0.1	200	0.3	77	80	300	100	$[-1,+1]$

3. Time-dependent Mechanical Loading

In this paper, we assume that angular velocity and acceleration as mechanical loading is a function of time (t), rather than a constant state as discussed in the previous literature [1-21]. For the convenience of modeling rotating disk in general form, angular velocity and acceleration are defined as an exponential function [17]:

$$\omega(t) = \omega_o e^{-\lambda t} \quad (4)$$

$$\dot{\omega}(t) = \frac{d\omega(t)}{dt} = -\lambda \omega_o e^{-\lambda t} \quad (5)$$

Such relations focus on the accelerating or decelerating process on the rotating disk. In these relations, ω_o is the initial angular velocity, and λ is a constant that influences the law of transition. If $\lambda > 0$, it is a decelerating process that occurs when the rotating disk decides to stop. While accelerating when $\lambda < 0$, in this situation the disk decides to start the work condition. If $\lambda = 0$, the disk is rotating with a constant angular velocity and zero angular acceleration, this situation is equal to normal work. Elastic limit angular velocity (ω_e) and elastic limit angular acceleration ($\dot{\omega}_e$) occurs when the von Mises stress as equivalent stress exceeds the yield strength of the material of disk.

In Fig. 3, the angular velocity and acceleration variations based on the parameters in Table 1 are plotted for various time values (t). As seen in these figures, for $\lambda > 0$, the changes in angular velocity and acceleration are completely different over time. The angular velocity is positive; it has ω_o value at $t=0$ and tends toward zero as time increases. But angular acceleration is negative; it has $-\omega_o \lambda$ value at $t=0$ and tends toward zero as time increases. For $\lambda = 0$, the angular velocity is constant over time ($\omega(t) = \omega_o$) and angular acceleration is zero. For $\lambda < 0$, changes in angular velocity and acceleration over time are similar.

4. Theoretical Background

4.1. Governing equation of rotating disk

In this part, assuming that the disk is thin, has a variable thickness which is a function of r and rotates around the z -axis with angular velocity and acceleration that is a function of time (t). Fig. 4 displays a disk element with all in-plane forces in the radial (r) and tangential (θ) directions of a polar coordinate system. The equilibrium equations can be given in relative directions as [12- 13, 17]:

$$\frac{d}{dr}[\sigma_r h(r)r] + \frac{d\tau_{r\theta}}{d\theta} h(r) - \sigma_\theta h(r) = -\rho(r)\omega^2 r^2 h(r) \quad (6)$$

$$\frac{d}{dr}[\tau_{r\theta} h(r)r] + \tau_{r\theta} h(r) = -\rho(r)\dot{\omega} r^2 h(r) \quad (7)$$

where $\rho(r)$ is density distribution function, ω is the angular velocity, $\dot{\omega}$ is the angular acceleration, $f(r) = -\rho(r)\omega^2 r^2 h(r)$ is a radial force, and $f(\theta) = -\rho(r)\dot{\omega} r^2 h(r)$ is a tangential force. Otherwise, σ_r and σ_θ are radial and tangential components of the normal stresses and $\tau_{r\theta}$ is the shear stress. Because of the rotational symmetry in this problem, displacements fields are functions of r only and Eqs. (6-7) can be simplified further to:

$$\frac{d}{dr}[\sigma_r h(r)r] - \sigma_\theta h(r) = -\rho(r)\omega^2 r^2 h(r) \quad (8)$$

$$\frac{d}{dr}[\tau_{r\theta}(r)h(r)r] + \tau_{r\theta}(r)h(r) = -\rho(r)\dot{\omega} r^2 h(r) \quad (9)$$

The stress-strain relationship in the plane stress and small deflection condition assumed for these analyses are [2]:

$$\sigma_r(r) = \frac{E}{1-\nu^2} [\varepsilon_r(r) + \nu \varepsilon_\theta(r)] \quad (10)$$

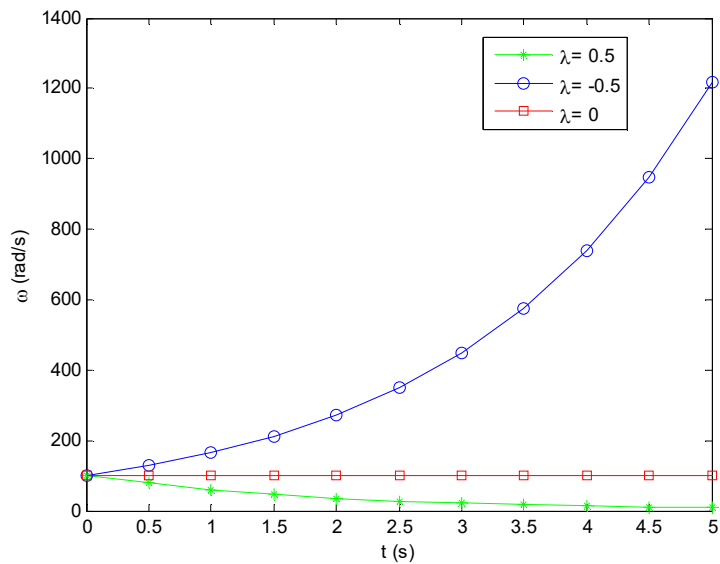
$$\sigma_\theta(r) = \frac{E}{1-\nu^2} [\varepsilon_\theta(r) + \nu \varepsilon_r(r)] \quad (11)$$

$$\tau_{r\theta}(r) = G\gamma_{r\theta} \quad (12)$$

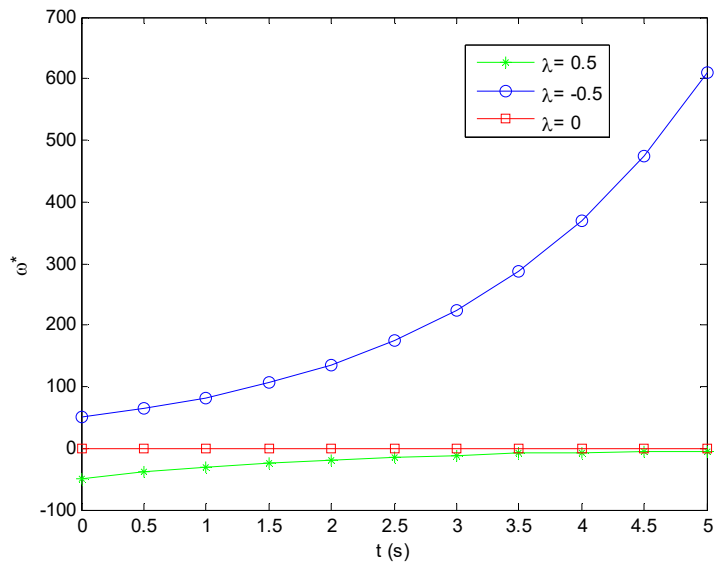
and strain-displacement relationships can be defined as:

$$\varepsilon_r(r) = \frac{du_r(r)}{dr} \quad (13)$$





(a)



(b)

Fig. 3. a) Angular velocity, b) Angular acceleration, for different value of λ

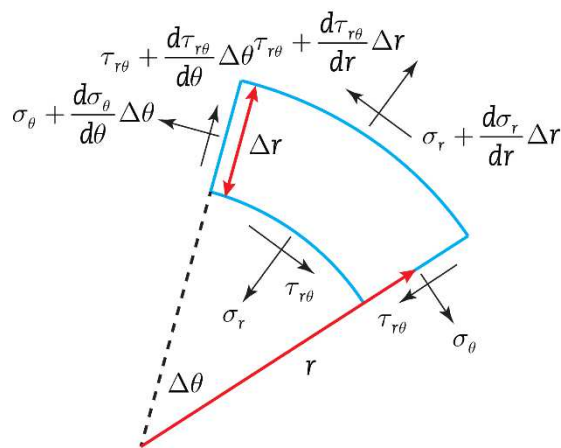


Fig. 4. Acting forces at the disk element [12-13]



$$\varepsilon_\theta(r) = \frac{u_r(r)}{r} + \frac{1}{r} \frac{du_\theta(r)}{d\theta} \xrightarrow{\text{Rotational symmetry}} \varepsilon_\theta(r) = \frac{u_r(r)}{r} \tag{14}$$

$$\gamma_{r\theta}(r) = \frac{1}{r} \frac{du_r(r)}{d\theta} + \frac{du_\theta(r)}{dr} - \frac{u_\theta(r)}{r} \xrightarrow{\text{Rotational symmetry}} \gamma_{r\theta}(r) = \frac{du_\theta(r)}{dr} - \frac{u_\theta(r)}{r} \tag{15}$$

with a substitution of Eqs. (10-12 and 13-15) in the relations (8 and 9), yields the following governing equation in the term of radial (u_r) and tangential (u_θ) displacements in relative direction:

$$\frac{d^2 u_r(r)}{dr^2} + \left[\frac{1}{r} + \frac{1}{h(r)} \frac{dh(r)}{dr} \right] \frac{du_r(r)}{dr} - \left[\frac{1}{r^2} - \frac{\nu}{h(r)r} \frac{dh(r)}{dr} \right] u_r(r) = - \frac{(1-\nu^2)\rho(r)\omega^2 r}{E} \tag{16}$$

$$\frac{d^2 u_\theta(r)}{dr^2} + \left[\frac{1}{r} + \frac{1}{h(r)} \frac{dh(r)}{dr} \right] \frac{du_\theta(r)}{dr} - \left[\frac{1}{r^2} + \frac{1}{h(r)r} \frac{dh(r)}{dr} \right] u_\theta(r) = - \frac{\rho(r)\dot{\omega} r}{G} \tag{17}$$

where, G is shear modulus and ν is the Poisson ratio. For mention, the analytical solution of the Eq. (16) for constant angular velocity by the Homotopy perturbation method, Variational iteration method, Adomian's decomposition method and Runge-Kutta method is shown in references [10, 12]. Such findings are in excellent agreement for thickness and density profile as $h(r) = h_0(r/b)^{-n}$, $\rho(r) = \rho_0(r/b)^m$. A new density profile is assumed in this study; HPM is implemented to solve equilibrium Eqs. (16 and 17) for angular velocity and acceleration that is changing over time.

4.2. Homotopy Perturbation Method (HPM) [22-26]

To present HPM, let us consider the following differential equation and boundary condition:

$$A(u) - f(r) = 0, \quad r \in \Theta, \tag{18}$$

$$B(u, \partial u / \partial n) = 0, \quad r \in \Gamma, \tag{19}$$

In this relation, u is the unknown function, A is a general differential operator, B is a boundary operator, $f(r)$ is a known analytic functional and Γ is the domain boundary. One of the most important steps in solving the differential equations by HPM is to find the linear and nonlinear parts of the function A . Hence, function A in Eq. (18) can be divided into two parts L and N . In this definition, L is a linear part whereas N is a nonlinear part. So, Eq. (18) rewritable as:

$$L(u) + N(u) - f(r) = 0. \tag{20}$$

The Homotopy perturbation structure is established as the following equation:

$$H(v, p) = L(v) - L(u_0) + pL(u_0) + p[N(v) - f(r)] = 0 \tag{21}$$

where v in HPM is a character variable by below definition:

$$v(r, p): \Theta \times [0, 1] \rightarrow R \tag{22}$$

At Eq. (21), $p \in [0, 1]$ is the embedding parameter and u_0 is the first approximation that satisfies the boundary condition in Eq. (19). For $p = 0$ and $p = 1$, Eq. (21) reduced to the following equations respectively:

$$H(v, 0) = L(v) - L(u_0) = 0, \quad H(v, 1) = A(v) - f(r) = 0 \tag{23}$$

This relation shows that $L(v) = L(u_0)$ and $A(v) = f(r)$. This information is used to writing Eq. (21). To begin the process of solving, we consider v as following:

$$v = v_0 + p v_1 + p^2 v_2 + p^3 v_3 + \dots \tag{24}$$

Then, Eq. (21) is arranged according to the various powers of p -terms (p^0, p^1, p^2, \dots). Each coefficient of p -terms is a differential equation in terms of variable v that must be solved. After this stage, the process of changes of p from zero to unity is that of $v(r, p)$ changing from u_0 to $u(r)$. And the best approximation for the solution is:

$$u = \lim_{p \rightarrow 1} v = v_0 + v_1 + v_2 + \dots \tag{25}$$

The above convergence is discussed in [22-26].

4.3. Finite Difference method (FDM) [27-28]

One of the effective methods for the numerical solutions of differential equations is the finite difference method. This approach is one of the easiest and the oldest methods to solve difficult or impossible differential equations. Finite difference approximation of derivatives plays a key function for the numerical solutions of differential equations in this method. The solution's precision depends on the number of grid points chosen. By increasing the number of grid points one can improve the precision of the solution to some desired degree. To solve differential equations with stated boundary conditions, a set of grid points must be identified in the variable interval. Central difference equations often approximate the derivatives of a function $f(r)$. But derivatives for grid point in boundary conditions are written based on the forward and backward finite difference form. Therefore, the first derivative concerning r in central-forward-backward difference form can be written as [27-28]:



$$\left. \frac{df}{dr} \right|^{r=r_i} \xrightarrow{\text{Central}} \frac{f^{i+1} - f^{i-1}}{2\delta_r} + O(h^2), \quad \left. \frac{df}{dr} \right|^{r=r_i} \xrightarrow{\text{Forward}} \frac{f^{i+1} - f^i}{\delta_r} + O(h), \quad \left. \frac{df}{dr} \right|^{r=r_i} \xrightarrow{\text{Backward}} \frac{f^i - f^{i-1}}{\delta_r} + O(h) \quad (26)$$

While the second derivative of a function $f(r)$ for r is:

$$\left. \frac{d^2f}{dr^2} \right|^{r=r_i} \xrightarrow{\text{Central}} \frac{f^{i+1} - 2f^i + f^{i-1}}{\delta_r^2} + O(h^2), \quad \left. \frac{d^2f}{dr^2} \right|^{r=r_i} \xrightarrow{\text{Forward}} \frac{f^{i+2} - 2f^{i+1} + f^i}{\delta_r^2} + O(h), \quad \left. \frac{d^2f}{dr^2} \right|^{r=r_i} \xrightarrow{\text{Backward}} \frac{f^i - 2f^{i-1} + f^{i-2}}{\delta_r^2} + O(h) \quad (27)$$

The references [26-27] include other finite-difference types of derivatives for a function $f(r)$. The differential equation is written in the finite difference form for each grid point in the interval $[0,1]$. In this scheme, the boundary conditions are written, too. Finally, the set of linear algebraic equations can be obtained in the following matrix expression which must be solved using an appropriate method [28].

$$A \cdot U = B \quad (28)$$

At the end of the finite difference process, there are $N-2$ equations for the inner points and two equations for the inner and outer surface boundary condition of the disk.

5. Analytical Solution

To achieve the analytical model, in this section elastic annular rotating disks with variable thickness and density are considered in its general form under variable mechanical loading. The equilibrium equations in both the radial and tangential directions are simultaneously solved by HPM as an analytical method to achieve this paper's goals.

5.1. Application of HPM

5.1.1. Radial direction

At first, the equilibrium equation is solved in a radial direction. Eqs. (1-2 and 4) are substituted into Eq. (16) and yields the following differential equation in term of unknown radial displacement:

$$\frac{d^2u_r(r)}{dr^2} + \left[\frac{(1-n)}{r} \right] \frac{du_r(r)}{dr} - \left[\frac{(1+nv)}{r^2} \right] u_r(r) = - \frac{(1-v^2)(\rho_0 + \rho_1 r + \rho_2 r^2 + \rho_3 r^3)(\omega_0 e^{-\lambda t})^2 r}{E} \quad (29)$$

Once the linear and nonlinear parts of this equation are separated according to the definitions for Eq. (21), HPM can be applied as:

$$L(u_{or}(r)) = \frac{d^2u_{or}(r)}{dr^2} + \left[\frac{(1-n)}{r} \right] \frac{du_{or}(r)}{dr} - \left[\frac{(1+nv)}{r^2} \right] u_{or}(r) \quad (30)$$

$$L(v(r)) = \frac{d^2v(r)}{dr^2} + \left[\frac{(1-n)}{r} \right] \frac{dv(r)}{dr} - \left[\frac{(1+nv)}{r^2} \right] v(r) \quad (31)$$

$$f(r) = - \frac{(1-v^2)(\rho_0 + \rho_1 r + \rho_2 r^2 + \rho_3 r^3)(\omega_0 e^{-\lambda t})^2 r}{E} \quad (32)$$

where $L(v(r))$ is the linear part of the Eq. (29) and $L(u_{or}(r))$ is its initial approximation. Due to the time dependence of the function $f(r)$, the equilibrium equation must be resolved at each loading step. But the displacement field is still only dependent on the variable r . We considered v as:

$$v(r) = v_0(r) + p v_1(r) + p^2 v_2(r) \quad (33)$$

Replacement Eqs. (30-32) into Eq. (21) and rearrangement based on the powers of p -terms, we have:

$$p^0: \quad \frac{u_{or}(r)}{r^2} + \frac{du_{or}(r)}{dr} \frac{n}{r} + \frac{dv_0(r)}{dr} \frac{1}{r} - \frac{d^2u_{or}(r)}{dr^2} - \frac{nv_0(r)}{r^2} + \frac{d^2v_0(r)}{dr^2} - \frac{v_0(r)}{r^2} - \frac{du_{or}(r)}{dr} \frac{1}{r} + \frac{nv_0(r)}{r^2} - \frac{dv_0(r)}{dr} \frac{n}{r} = 0 \quad (34)$$

$$p^1: \quad - \frac{u_{or}(r)}{r^2} + \frac{d^2v_1(r)}{dr^2} + \frac{d^2u_{or}(r)}{dr^2} + \frac{du_{or}(r)}{dr} \frac{1}{r} - \frac{nv_1(r)}{r^2} - \frac{dv_1(r)}{dr} \frac{n}{r} - \frac{v_1(r)}{r^2} + \frac{dv_1(r)}{dr} \frac{1}{r} - \frac{nv_0(r)}{r^2} - \frac{du_{or}(r)}{dr} \frac{n}{r} + \frac{(1-v^2)(\rho_0 + \rho_1 r + \rho_2 r^2 + \rho_3 r^3)(\omega_0 e^{-\lambda t})^2 r}{E} = 0 \quad (35)$$

$$p^2: \quad - \frac{dv_2(r)}{dr} \frac{n}{r} - \frac{nv_2(r)}{r^2} + \frac{d^2v_2(r)}{dr^2} - \frac{v_2(r)}{r^2} + \frac{dv_2(r)}{dr} \frac{1}{r} = 0 \quad (36)$$

The above equations are to be solved to determine function v . Solving Eq. (34), we have:

$$v_0(r) = u_{or}(r) = C_1 r^{\frac{1}{2}n + \frac{1}{2}\sqrt{n^2 + 4nv + 4}} + C_2 r^{\frac{1}{2}n - \frac{1}{2}\sqrt{n^2 + 4nv + 4}} \quad (37)$$

Similarly, solving Eqs. (35 and 36) yields the following results respectively:



$$v_1(r) = C_1 r^{\frac{1}{2}n + \frac{1}{2}\sqrt{n^2 + 4nv + 4}} + C_2 r^{\frac{1}{2}n - \frac{1}{2}\sqrt{n^2 + 4nv + 4}} + \frac{(1 - \nu^2)(\omega_0 e^{-\lambda t})^2 r^3}{(nv + 5n - 24)(nv + 3n - 8)(nv + 6n - 35)(nv + 4n - 15)E}$$

$$\left[(-12600 + (1725\nu + 8145)n - (74\nu^2 + 720\nu + 1726)n^2 + (\nu^3 + 15\nu^2 + 74\nu + 120)n^3) \rho_0 + \left(\frac{-6720 + (1312\nu + 5072)n - (67\nu^2 + 584\nu + 1197)n^2 + (\nu^3 + 14\nu^2 + 63\nu + 90)n^3}{(47\nu^2 + 360\nu + 673)n^2 + (\nu^3 + 12\nu^2 + 47\nu + 60)n^3} \right) r \rho_1 + \right. \quad (38)$$

$$\left. (-4200 + (925\nu + 3415)n - (58\nu^2 + 460\nu + 882)n^2 + (\nu^3 + 13\nu^2 + 54\nu + 72)n^3) r^2 \rho_2 + \left(\frac{-2880 + (672\nu + 2448)n - (47\nu^2 + 360\nu + 673)n^2 + (\nu^3 + 12\nu^2 + 47\nu + 60)n^3}{(47\nu^2 + 360\nu + 673)n^2 + (\nu^3 + 12\nu^2 + 47\nu + 60)n^3} \right) r^3 \rho_3 \right]$$

$$v_2(r) = C_1 r^{\frac{1}{2}n + \frac{1}{2}\sqrt{n^2 + 4nv + 4}} + C_2 r^{\frac{1}{2}n - \frac{1}{2}\sqrt{n^2 + 4nv + 4}} \quad (39)$$

Replacement of the above equations (37-39) in Eq. (33) gives the equation for v and as $p \rightarrow 1$, then $v(r) \xrightarrow{\text{yields}} u_r(r)$. That means finding the answer for the governing equation of elastic rotating disk (i.e., Eq. (16)) in the general form of non-uniform thickness and density. The optimum number of HPM iteration considering the converged result is two. Therefore, the semi-exact solution of $u_r(r)$ is:

$$u_r(r) = C_1 r^{\frac{1}{2}n + \frac{1}{2}\sqrt{n^2 + 4nv + 4}} + C_2 r^{\frac{1}{2}n - \frac{1}{2}\sqrt{n^2 + 4nv + 4}} + \frac{(1 - \nu^2)(\omega_0 e^{-\lambda t})^2 r^3}{(nv + 5n - 24)(nv + 3n - 8)(nv + 6n - 35)(nv + 4n - 15)E}$$

$$\left[(-12600 + (1725\nu + 8145)n - (74\nu^2 + 720\nu + 1726)n^2 + (\nu^3 + 15\nu^2 + 74\nu + 120)n^3) \rho_0 + \left(\frac{-6720 + (1312\nu + 5072)n - (67\nu^2 + 584\nu + 1197)n^2 + (\nu^3 + 14\nu^2 + 63\nu + 90)n^3}{(47\nu^2 + 360\nu + 673)n^2 + (\nu^3 + 12\nu^2 + 47\nu + 60)n^3} \right) r \rho_1 + \right. \quad (40)$$

$$\left. (-4200 + (925\nu + 3415)n - (58\nu^2 + 460\nu + 882)n^2 + (\nu^3 + 13\nu^2 + 54\nu + 72)n^3) r^2 \rho_2 + \left(\frac{-2880 + (672\nu + 2448)n - (47\nu^2 + 360\nu + 673)n^2 + (\nu^3 + 12\nu^2 + 47\nu + 60)n^3}{(47\nu^2 + 360\nu + 673)n^2 + (\nu^3 + 12\nu^2 + 47\nu + 60)n^3} \right) r^3 \rho_3 \right]$$

In this relation, C_1 and C_2 are integration constants to be calculated by applying boundary conditions on both inner and outer surfaces. As shown on Eq. (40), radial displacement is a function of the thickness parameter (n), the Poisson ratio (ν), the Young modulus (E), the constant parameters in the density function ($\rho_0, \rho_1, \rho_2, \rho_3$), the initial angular velocity (ω_0), the constant (λ) and the variable time (t).

5.1.2. Tangential direction

In this section, HPM solves the equilibrium equation in the tangential direction. This equilibrium equation is obtained with the substitution of Eqs. (1-2 and 4) into Eq. (17) as follow:

$$\frac{d^2 u_\theta(r)}{dr^2} + \left[\frac{(1-n)}{r} \right] \frac{du_\theta(r)}{dr} - \left[\frac{(1-n)}{r^2} \right] u_\theta(r) = - \frac{(\rho_0 + \rho_1 r + \rho_2 r^2 + \rho_3 r^3)(-\lambda \omega_0 e^{-\lambda t}) r}{G} \quad (41)$$

After the linear and nonlinear parts of this equation are separated, HPM can be defined as:

$$L(v(r)) = \frac{d^2 v(r)}{dr^2} + \left[\frac{(1-n)}{r} \right] \frac{dv(r)}{dr} - \left[\frac{(1-n)}{r^2} \right] v(r) \quad (42)$$

$$L(u_{0\theta}(r)) = \frac{d^2 u_{0\theta}(r)}{dr^2} + \left[\frac{(1-n)}{r} \right] \frac{du_{0\theta}(r)}{dr} - \left[\frac{(1-n)}{r^2} \right] u_{0\theta}(r) \quad (43)$$

$$f(r) = - \frac{(\rho_0 + \rho_1 r + \rho_2 r^2 + \rho_3 r^3)(-\lambda \omega_0 e^{-\lambda t}) r}{G} \quad (44)$$

Where $L(v(r))$ is the linear part of the Eq. (41) and $L(u_{0\theta}(r))$ is its initial approximation. We considered v as its definition in Eq. (33). With substituting Eqs. (42-44) into Eq. (21) and rearrangement on the basis of p -terms components, we have:

$$p^0 : \frac{u_{0\theta}(r)}{r^2} + \frac{du_{0\theta}(r)}{dr} \frac{n}{r} + \frac{dv_0(r)}{dr} \frac{1}{r} - \frac{d^2 u_{0\theta}(r)}{dr^2} + \frac{nv_0(r)}{r^2} + \frac{d^2 v_0(r)}{dr^2} - \frac{v_0(r)}{r^2} - \frac{du_{0\theta}(r)}{dr} \frac{1}{r} - \frac{nu_{0\theta}(r)}{r^2} - \frac{dv_0(r)}{dr} \frac{n}{r} = 0 \quad (45)$$

$$p^1 : - \frac{u_{0\theta}(r)}{r^2} + \frac{d^2 v_1(r)}{dr^2} + \frac{d^2 u_{0\theta}(r)}{dr^2} + \frac{du_{0\theta}(r)}{dr} \frac{1}{r} + \frac{nv_1(r)}{r^2} - \frac{dv_1(r)}{dr} \frac{n}{r} - \frac{v_1(r)}{r^2} + \frac{dv_1(r)}{dr} \frac{1}{r} + \frac{nu_{0\theta}(r)}{r^2} - \frac{du_{0\theta}(r)}{dr} \frac{n}{r} + \frac{(\rho_0 + \rho_1 r + \rho_2 r^2 + \rho_3 r^3)(-\lambda \omega_0 e^{-\lambda t}) r}{G} = 0 \quad (46)$$

$$p^2 : \frac{dv_2(r)}{dr} \frac{1}{r} + \frac{nv_2(r)}{r^2} + \frac{d^2 v_2(r)}{dr^2} - \frac{v_2(r)}{r^2} - \frac{d^2 v_2(r)}{dr} \frac{n}{r} = 0 \quad (47)$$

To determine v function, the above equations are to be solved. Solving Eq. (45), we have:

$$v_0(r) = u_{0\theta}(r) = C_3 r + C_4 r^{(n-1)} \quad (48)$$

Similarly, solving Eqs. (46 and 47) respectively give the following results:



$$v_1(r) = C_3 r + C_4 r^{(n-1)} + \frac{1}{60} \frac{(-\lambda \omega_0 e^{-\lambda t}) r^3}{(n-4)(n-5)(n-6)(n-7)G} [(-6300 + 3210n - 540n^2 + 30n^3) \rho_0 + (-3360 + 1880n - 340n^2 + 20n^3) r \rho_1 + (-2100 + 1245n - 240n^2 + 15n^3) r^2 \rho_2 + (-1440 + 888n - 180n^2 + 12n^3) r^3 \rho_3] \quad (49)$$

$$v_2(r) = C_3 r + C_4 r^{(n-1)} \quad (50)$$

Substitution equations (48-50) in Eq. (33) includes the equation for v and as $p \rightarrow 1$, then $v(r) \rightarrow u_\theta(r)$. This means finding the answer for Eq. (17) in the general form of non-uniform thickness and density. In this case, the optimum number of HPM iteration is two when with considering the converged result and the exact solution of $u_\theta(r)$ is:

$$u_\theta(r) = C_3 r + C_4 r^{(n-1)} + \frac{1}{60} \frac{(-\lambda \omega_0 e^{-\lambda t}) r^3}{(n-4)(n-5)(n-6)(n-7)G} [(-6300 + 3210n - 540n^2 + 30n^3) \rho_0 + (-3360 + 1880n - 340n^2 + 20n^3) r \rho_1 + (-2100 + 1245n - 240n^2 + 15n^3) r^2 \rho_2 + (-1440 + 888n - 180n^2 + 12n^3) r^3 \rho_3] \quad (51)$$

Tangential displacement in Eq. (51) is a function of the thickness parameter (n), the shear modulus (G), the constant parameters in the density function ($\rho_0, \rho_1, \rho_2, \rho_3$), the initial angular velocity (ω_0), the constant (λ) and the variable time (t). In this relation, C_3 and C_4 are integrations constant to be determined by applying boundary conditions of rotating disk at inner and outer surfaces. Two various types of boundary conditions are considered in this paper.

6. Numerical Solution

6.1. Application of FDM

The differential Eqs. (16 and 17) is valid for elastic deformations of non-uniform thickness and density rotating disk under variable mechanical load in radial and tangential direction. Derivatives of the displacement component in the radial direction are replaced by Eqs. (26-27) to solve the differential equation by finite difference method. Finally, these differential equations express in the form of finite difference as follows:

$$\frac{u_r^{i+1} - 2u_r^i + u_r^{i-1}}{\delta_r^2} + \frac{(1-n)u_r^{i+1} - u_r^{i-1}}{r_i} - \frac{(1+nv)u_r^i}{r_i^2} = -\frac{(1-v^2)(\rho_0 + \rho_1 r_i + \rho_2 r_i^2 + \rho_3 r_i^3)(\omega_0 e^{-\lambda t})^2 r_i}{E} \quad (52)$$

$$\frac{u_\theta^{i+1} - 2u_\theta^i + u_\theta^{i-1}}{\delta_r^2} + \frac{(1-n)u_\theta^{i+1} - u_\theta^{i-1}}{r_i} - \frac{(1-n)u_\theta^i}{r_i^2} = -\frac{(\rho_0 + \rho_1 r_i + \rho_2 r_i^2 + \rho_3 r_i^3)(-\lambda \omega_0 e^{-\lambda t}) r_i}{G} \quad (53)$$

The radial direction of the disk ($r \in [r_i, r_e]$) is divided to N grid points ($i = [1, N]$). The FD form of differential equations is written for internal grid points. The boundary condition of the rotating disk at the inner and outer surfaces of the disk must also be represented in the FD form. The FD form of two different boundary conditions is:

(a) Radially restricted and directed boundary conditions: if the inner surface of the annular disk is placed on a rigid shaft and the outer surface is directed as shown in Fig.1, the FD form of these boundary conditions are:

$$\text{Radial direction: } \begin{cases} i=1, & u_r(r_i) = 0 \rightarrow u_r^i = 0 \\ i=N, & u_r(r_e) = 0 \rightarrow u_r^i = 0 \end{cases} \quad \text{Tangential direction: } \begin{cases} i=1, & u_\theta(r_i) = 0 \rightarrow u_\theta^i = 0 \\ i=N, & u_\theta(r_e) = 0 \rightarrow u_\theta^i = 0 \end{cases} \quad (54)$$

(b) Radially restricted and free boundary conditions: if the annular disk is mounted placed on a rigid shaft and the outer surface is free of any traction, the FD form of these boundary conditions are:

$$\text{Radial direction: } \begin{cases} i=1, & u_r(r_i) = 0 \rightarrow u_r^i = 0 \\ i=N, & \sigma_r(r_e) = 0 \rightarrow \frac{E}{(1-v^2)} \left(\frac{du_r(r)}{dr} + \frac{v u_r(r)}{r} \right) = 0 \rightarrow \frac{u_r^i - u_r^{i-1}}{\delta_r} + \frac{v u_r^i}{r_i} = 0 \end{cases} \quad (55)$$

$$\text{Tangential direction: } \begin{cases} i=1, & u_\theta(r_i) = 0 \rightarrow u_\theta^i = 0 \\ i=N, & \tau_{r\theta}(r_e) = 0 \rightarrow \frac{1}{G} \left(\frac{du_\theta(r)}{dr} - \frac{u_\theta(r)}{r} \right) = 0 \rightarrow \frac{u_\theta^i - u_\theta^{i-1}}{\delta_r} - \frac{u_\theta^i}{r_i} = 0 \end{cases}$$

Eventually, a system of linear algebraic equations is achieved. The radial and tangential displacement of the rotating disk for each grid point is determined by solving the system of equations.

7. Results and Discussions

7.1. Verification of HPM

The geometry and material properties used for the disks in this research are listed in Table 1. This section's main objective is to demonstrate the ability of the HPM to manage non-uniform thickness and density rotating disks taking into consideration angular velocity and acceleration that varies in simulations over time. It's quite interesting to note that the exact solution of the Eqs. (16) and (17) for uniform thickness and density rotating disk with constant angular velocity (ω) and acceleration ($\dot{\omega}$) can be



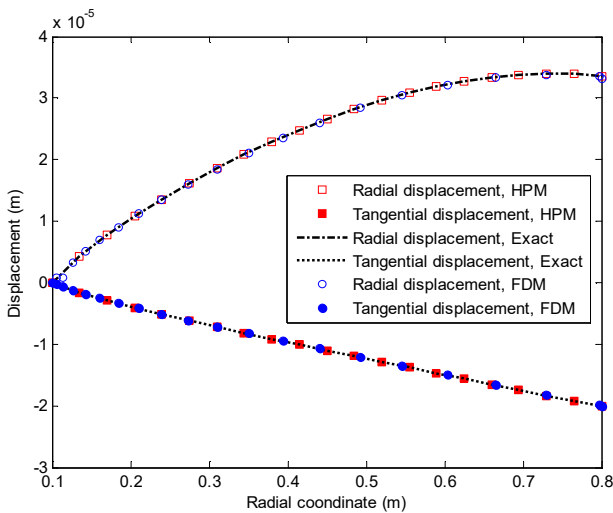
shown as [12, 29]:

$$u_r(r) = C_1 r + \frac{C_2}{r} - \frac{(1-\nu^2)\rho_0\omega^2 r^3}{8E} \tag{56}$$

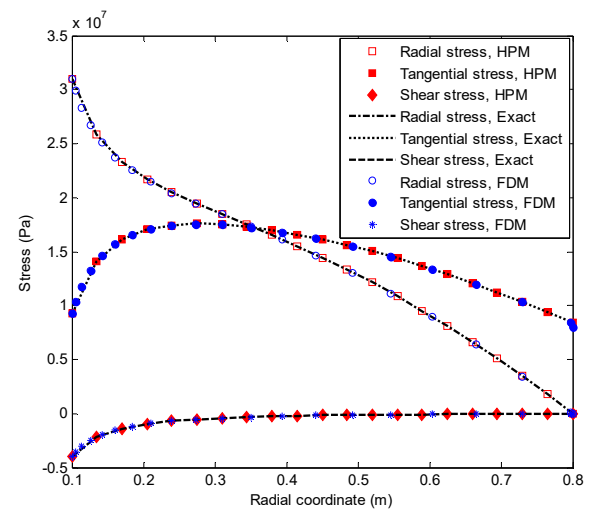
$$u_\theta(r) = \frac{C_3}{2Gr} - C_4 r - \frac{\rho\omega r^3}{8G} \tag{57}$$

In Finite difference method, for solving equilibrium equations in the FD form as Eqs. (52-53) and to increase the accuracy of the solutions, the radial distance, $(r_e - r_i)$ is divided into N steps, $\delta_r = (r_e - r_i) / N$. Also, a mesh sensitivity analysis was performed to ensure that the results are independent on the mesh size, and N was set to 401.

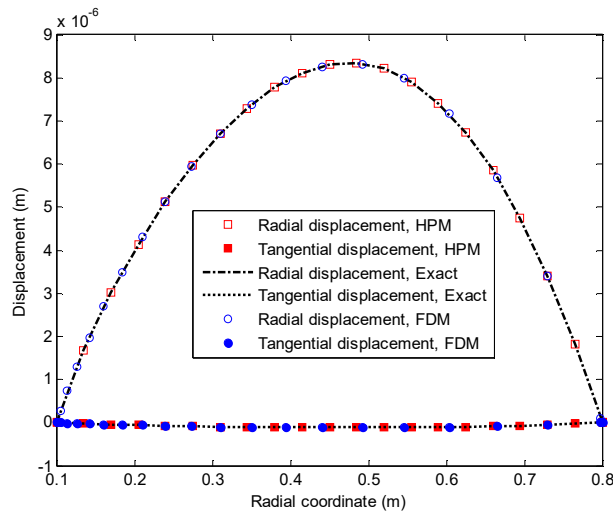
For the case of uniform thickness and density, Fig. 5 compares the HPM and FDM results for both radial and tangential displacements-stress distributions. In this figure, the angular velocity and acceleration assumed constant, hence the affected parameter in Eqs. (4 and 5) is considered zero ($t = 0$). So, the finding is shown in Fig. 5 are based on the $\omega|_{t=0} = \omega_0 = 100\text{rad/s}$ and $\dot{\omega}|_{t=0} = -\lambda\omega_0 \rightarrow \omega = -50\text{rad/s}^2$. Radially restricted-directed and radially restricted-free as boundary conditions are implemented, and HPM and FDM results are compared with those results obtained from the exact solution in Eqs. (56-57). As can be seen in this figure, the agreement between the results of HPM and FDM solutions for a uniform disk is excellent in comparison with the exact solution. Boundary conditions are completely satisfied. For radially restricted-free conditions, all of the radial and tangential displacements at the outer radius of a disk ($r = r_e$) have a maximum value. The radial and shear stress is achieved by their maximum values at the inner surface ($r = r_i$). The highest values of tangential stress do not exist in the disk's inner or outer surface, but occurs in the middle of the disk.



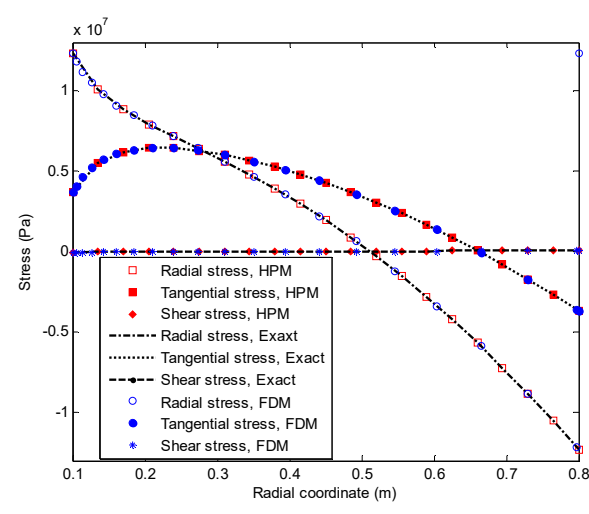
(a) Radially restricted-free: displacements



(a) Radially restricted-free: stresses



(b) Radially restricted-directed: displacements



(b) Radially restricted-directed: stresses

Fig. 5. Comparison of results for uniform thickness and density rotating disk: $t = 0, \lambda = 0.5$



The highest value of radial displacement occurs approximately in the center of the disk for radially restricted-directed conditions and its value is very high compared to tangential displacement. The maximum value of tangential stress also occurs approximately in the middle of the disk. The radial and shear stress reaches maximum values at both the inner and outer surface of the disk. This stress is positive at the inner surface, but it is negative on the disk's outer surface. There is a point along the radial direction of a disk with this boundary condition that has zero stresses. The level of displacement and stress in the disk with the radially restricted-directed condition is less than disk with the radially restricted-free conditions. This implies that for the disk with restricted-directed boundary conditions, the elastic limit of the angular velocity at which yielding starts is higher than disk with restricted-free boundary conditions.

To check the results of HPM for displacement-stress distribution in a rotating disk with non-uniform thickness and density, the thickness parameter in Eq. (1) is selected as $n=0.5$. The results are compared with the FDM solution in Fig. 6 for two prescribed boundary conditions. All the reported results are based on the use of constant angular velocity and acceleration ($\omega(@t=0) = \omega_0 = 100 \text{ rad/s}$ and $\dot{\omega}(@t=0) = -\lambda\omega_0 \rightarrow \dot{\omega} = -50 \text{ rad/s}^2$) and density function according to Eq. (2). It is important to note that there is no exact solution for rotating disks with non-uniform thickness and density. This figure shows the ability of these techniques to solve the governing equation of rotating disk at radial and tangential directions in its general form. In HPM, two iterations lead to the high precision of the solution in its general form (non-uniform thickness and density) for the governing equation of the problem. This solution is in good agreement with the results of both the exact and the FDM. The results show that HPM doesn't require specific algorithms, complex calculations, or large computational capacity, it is much simpler and straighter. By comparing Figs. 5 and 6, it can be seen that by considering the non-uniform thickness and density in a rotating disk, the level of tangential displacement and shear stress decreases as opposed to uniform disk at each affected point of the disk. For both boundary conditions, the distribution conditions of radial and tangential displacement are close to the uniform disk. But, unlike the uniform disk, values of radial and shear stress on the disk's inner and outer surfaces are not equal for the restricted-directed condition. These stresses reach its maximum value at the outer surface. It can be said that the factors that contribute to these results are the type of boundary conditions on disks.

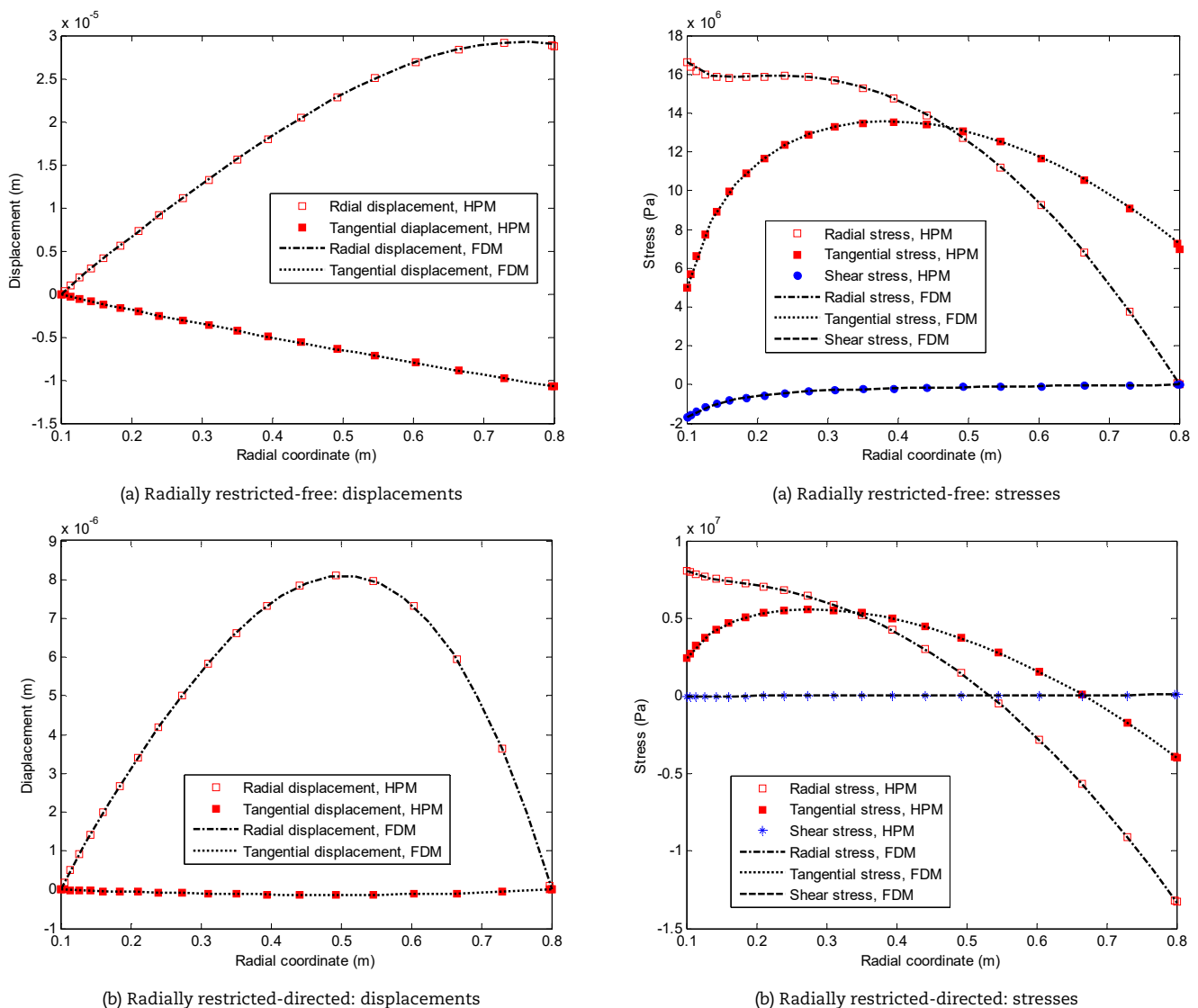


Fig. 6. Comparison of results for rotating an annular disk with thickness parameter $n = 0.5$ and $\rho(r) : t = 0, \lambda = 0.5$



7.2. Numerical results

Numerical examples are used in this section, to demonstrate the implementation of the presented analytical model.

7.2.1. Example 1

Parametric analysis is done in Fig. 7 for distributions of radial, tangential and shear stress for various thickness parameter n and constant in angular velocity function λ . Such results can be used to estimate the von Mises equivalent stress along the radius of the disk and identify its effective factors. All of the findings presented in Fig. 7 are calculated in time ($t = 2s$). At this time, deformations are still elastic in the rotating disks. According to Eqs. (3 and 4), If $\lambda = 0.5$ is considered, angular velocity and acceleration are estimated as ($\omega = 36.78 \text{ rad/s}$ and $\dot{\omega} = -18.39 \text{ rad/s}^2$). If $\lambda = -0.5$ is considered, these variables are estimated as ($\omega = 271.82 \text{ rad/s}$ and $\dot{\omega} = 135.91 \text{ rad/s}^2$). The decelerating effect of constant λ on these calculations is quite obvious. Its angular velocity and acceleration approaches to zero when $\lambda = 0.5$ and $t = 2s$ is considered. As shown at Fig. 7, the levels of shear stress compared to other stresses are low for both boundary conditions. As the thickness parameter increases, the level of these stresses is decreased. From Fig. 7 the maximum location of radial, tangential and shear stress for different values of the effective parameters n and λ are available.

7.2.2. Example 2

In this example, the von Mises stress distribution along the radial direction of a disk are discussed for various values of thickness parameter n and constant λ . The findings are illustrated based on two different boundary conditions in Fig. 8. As seen in this figure, for each boundary condition and for $\lambda > 0$, von Mises stress along the radius of disk trends to zero to stop the disk as time increases. In the case of $\lambda < 0$, von Mises stress levels increase rapidly as time increases. For radially restricted-free conditions and $\lambda < 0$, the maximum values of von Mises stress for thickness parameter $0 \leq n \leq 0.5$ occurs at the inner radius of a disk ($r = r_i$) and for the rest of the thickness parameter in the center of the disk approximately. In this case, the value of maximum von Mises stress is also decreasing as the thickness parameter increases. But the maximum values of this stress for all thickness parameters n occurs at the outer radius of a disk ($r = r_e$) for radially restricted-directed conditions and $\lambda < 0$. In this case, the combination of radial, tangential, and shear stress on the disk's outer surface is such that as a thickness parameter increases, the value of maximum von Mises stress is increasing.

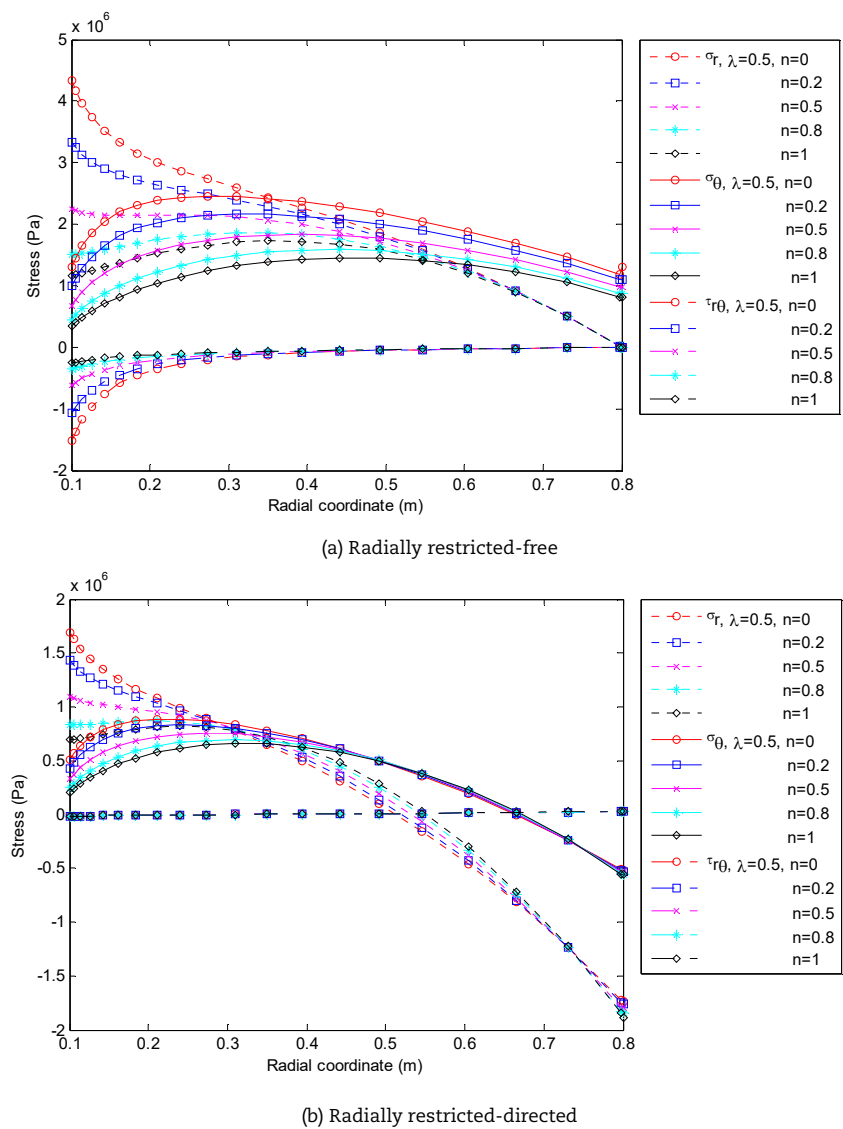


Fig. 7. Comparison of results for stresses in rotating disk with different thickness parameter n and $\rho(r) : t = 2s, \lambda = \pm 0.5$



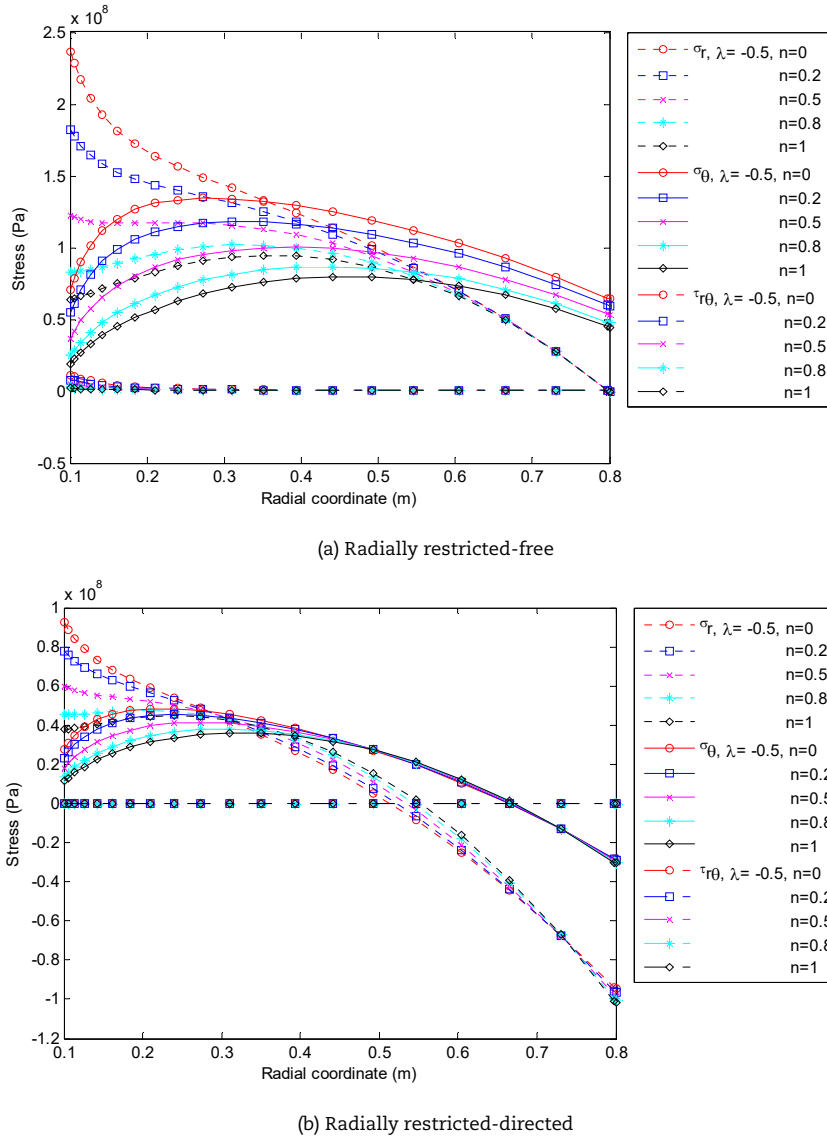


Fig. 7. Comparison of results for stresses in rotating disk with different thickness parameter n and $\rho(r)$: $t = 2s, \lambda = \pm 0.5$

7.2.3. Example 3

In this example, the effect of shear stress on calculations of equivalent von Mises stress is discussed. The von Mises equivalent stress is used as a criterion for evaluating the elastic limit angular velocity and acceleration. For rotating disks that are in-plane stress conditions, Von Mises stress is determined on the basis of the following relation as a criterion for initiating plastic deformations:

$$\sigma_{eq} = \sqrt{\sigma_r^2 + \sigma_\theta^2 - \sigma_r\sigma_\theta + 3\tau_{r\theta}^2} \tag{58}$$

It is known that if tangential deformation is eliminated, von Mises stress is obtained from the following equation. In this case, the radial and tangential stresses are the principal stresses.

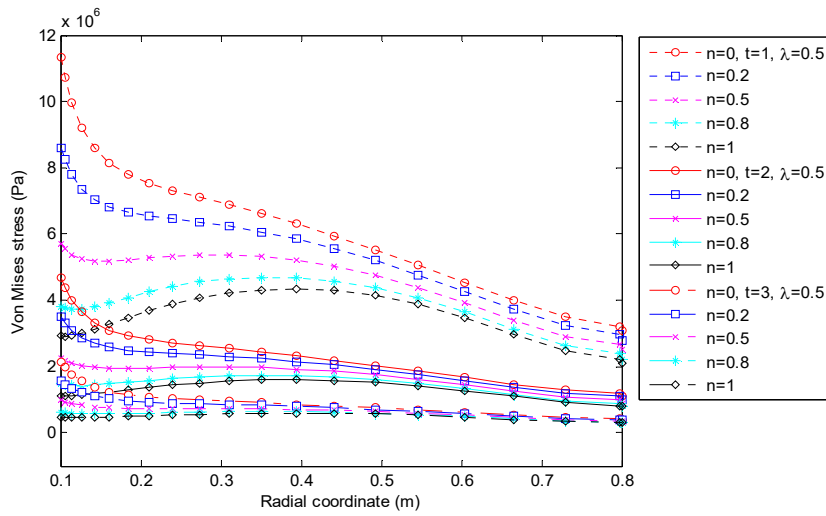
$$\sigma_{eq} = \sqrt{\sigma_r^2 + \sigma_\theta^2 - \sigma_r\sigma_\theta} \tag{59}$$

For clarity and for two specified boundary conditions, the distribution of von Mises stress along the radius of a disk for various values of thickness parameter n and constant ($\lambda = -0.5$) at a time ($t = 5s$) is demonstrated in Fig.9. As seen in this figure, the maximum values of von Mises stress at this time for some of the thickness parameters exceed the yield strength of the disk material and this disk with this thickness parameter undergoes plastic deformations. As seen in example 2, for radially restricted-free conditions, for some of the thickness parameters the maximum value of von Mises stress occurs in the inner surface and for the rest of thickness parameters in the middle of the radial direction of the disk. But the value of von Mises stress is maximum at the disk's outer surface for radially restricted-directed conditions. The location of maximum von Mises stress is important because plastic deformation initiated from this place.

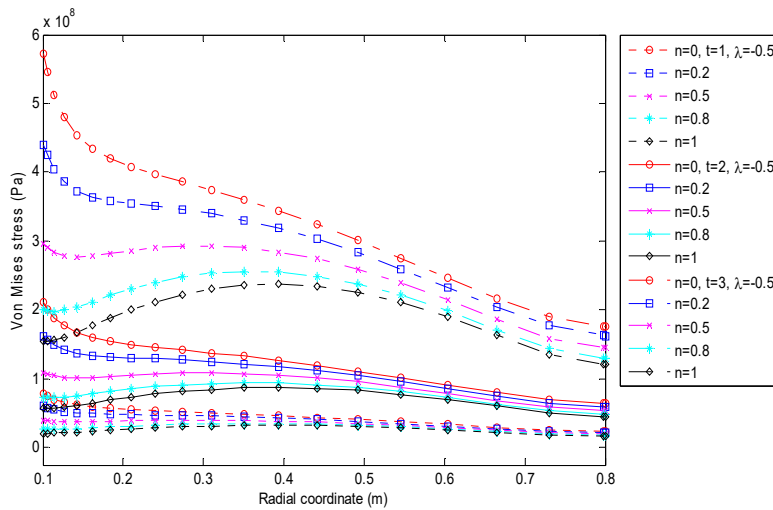
In the following, the values of maximum von Mises stress and radius with this maximum stress are prepared in Tables 2-4, with and without considering shear stress in calculations. The results are reported for various values of thickness parameter n , constant λ and two boundary conditions at the time ($t = 5s$). In these tables, the values of angular velocity and acceleration are estimated for any combination of constant λ and time t . As seen, the effect of shear stress in calculating maximum von Mises stress decreases by increasing the thickness parameter n for each value of constant λ . Furthermore, the effect of shear stress on



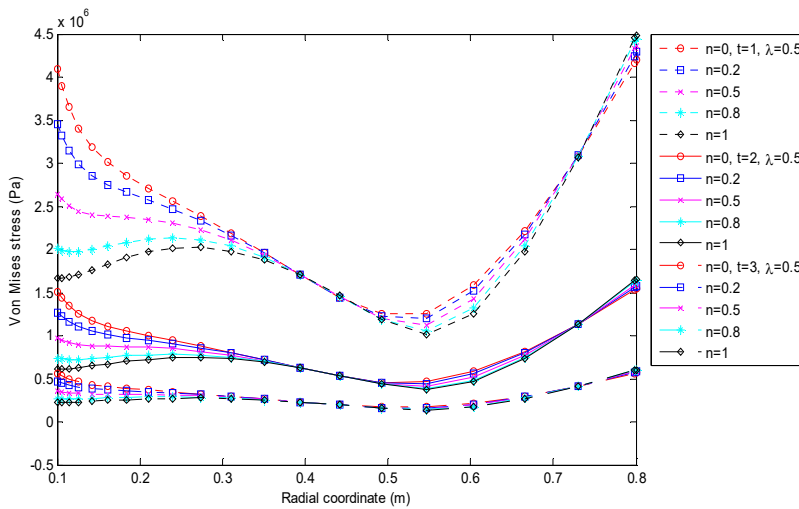
the disk with the radially restricted-free condition in this case is much greater than disk with the radially restricted-directed condition. In general and regardless of the type of boundary conditions on the disk, with considering the lower value of constant λ , the effect of shear stress in calculating maximum von Mises stress is increased. The lower value of constant λ is equivalent to having lower values of angular velocity and acceleration. It can be concluded that consideration of shear stress in the calculation of maximum von Mises stress is important, especially in the region of elastic deformation and must be considered for prediction of elastic limit angular velocity and acceleration.



(a) Radially restricted-free



(b) Radially restricted-directed



(a) Radially restricted-free

Fig. 8. Comparison of results for von Mises stress distribution of rotating disk with different thickness parameter n , constant λ , time t and $\rho(r)$



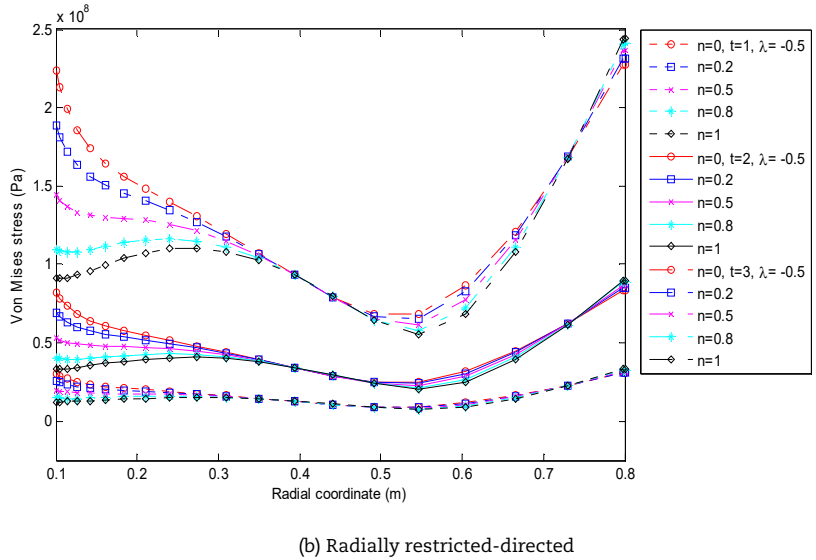


Fig. 8. Comparison of results for von Mises stress distribution of rotating disk with different thickness parameter n , constant λ , time t and $\rho(r)$

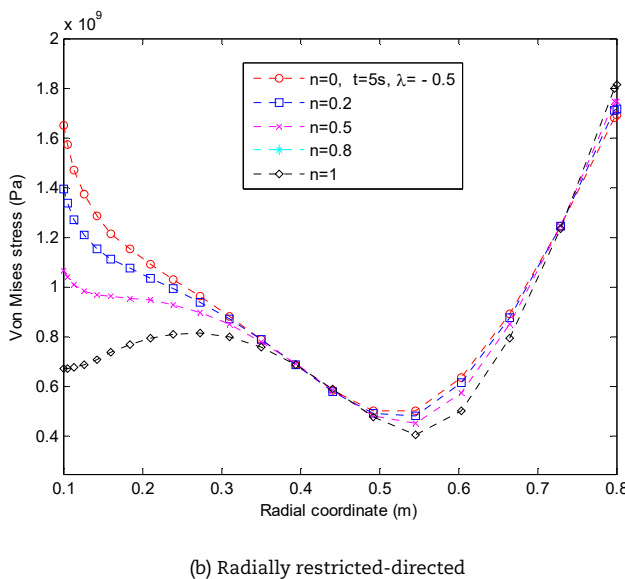
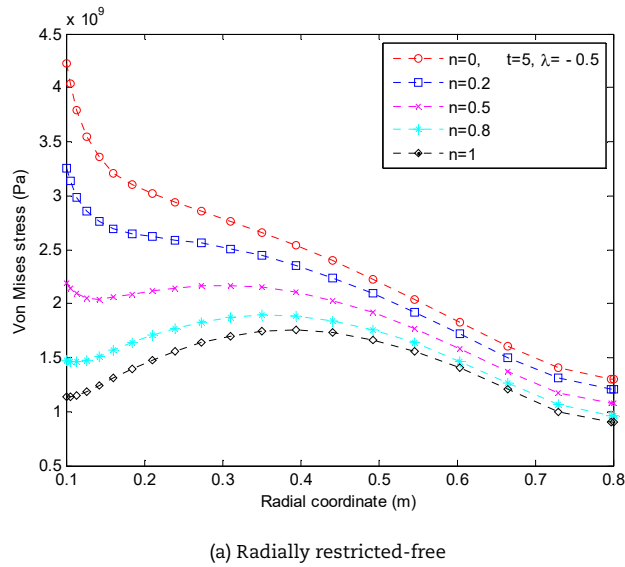


Fig. 9. Comparison of results for von Mises stress distribution of rotating an annular disk with different thickness parameter n and $\rho(r) : t = 5s, \lambda = -0.5$



Table 2. Results for maximum von Mises stress, a different value of thickness parameter n , $\lambda = -0.5$ at time $t = 5s$.

Angular velocity $\omega _{t=5, \lambda=-0.5} = 1218.2 \text{ rad/s}$		Angular acceleration $\dot{\omega} _{t=5, \lambda=-0.5} = 609.1 \text{ rad/s}^2$			
Thickness parameter (n)	Boundary conditions	Radius with maximum von Mises stress (r)	Von Mises stress with considering shear stress (MPa)	Von Mises stress without considering shear stress (Mpa)	Percent
0	Restricted-free	$r=0.1$	4223.1	4222.2	0.021%
	Restricted-directed	$r=0.6$	1692.16	1692.15	0.000031%
0.2	Restricted-free	$r=0.1$	3250.9	3250.3	0.017%
	Restricted-directed	$r=0.6$	1721.1	1721.1	0.000033%
0.5	Restricted-free	$r=0.1$	2190.0	2189.8	0.012%
	Restricted-directed	$r=0.6$	1760.3	1760.3	0.000037%
0.8	Restricted-free	$r=0.359$	1893.2	1893.1	0.00023%
	Restricted-directed	$r=0.6$	1794.5	1794.5	0.00004%
1	Restricted-free	$r=0.386$	1753.1	1753.1	0.00017%
	Restricted-directed	$r=0.6$	1814.6	1814.6	0.000043%

Table 3. Results for maximum von Mises stress, a different value of thickness parameter n , $\lambda = -0.35$ at time $t = 5s$.

Angular velocity $\omega _{t=5, \lambda=-0.35} = 575.4 \text{ rad/s}$		Angular acceleration $\dot{\omega} _{t=5, \lambda=-0.35} = 201.4 \text{ rad/s}^2$			
Thickness parameter (n)	Boundary conditions	Radius with maximum von Mises stress (r)	Von Mises stress with considering shear stress (MPa)	Von Mises stress without considering shear stress (Mpa)	Percent
0	Restricted-free	$r=0.1$	942.56	942.12	0.0471%
	Restricted-directed	$r=0.6$	377.572	377.571	0.00007%
0.2	Restricted-free	$r=0.1$	725.52	725.25	0.0383%
	Restricted-directed	$r=0.6$	384.0318	384.0315	0.000074%
0.5	Restricted-free	$r=0.1$	488.75	488.61	0.0285%
	Restricted-directed	$r=0.6$	392.7807	392.7804	0.000081%
0.8	Restricted-free	$r=0.359$	422.596	422.594	0.000521%
	Restricted-directed	$r=0.1$	400.4115	400.4111	0.000089%
1	Restricted-free	$r=0.386$	391.192	391.190	0.00039%
	Restricted-directed	$r=0.6$	404.907	404.906	0.000096%

Table 4. Results for maximum von Mises stress, a different value of thickness parameter n , $\lambda = -0.2$ at time $t = 5s$.

Angular velocity $\omega _{t=5, \lambda=-0.2} = 271.8 \text{ rad/s}$		Angular acceleration $\dot{\omega} _{t=5, \lambda=-0.2} = 54.3 \text{ rad/s}^2$			
Thickness parameter (n)	Boundary conditions	Radius with maximum von Mises stress (r)	Von Mises stress with considering shear stress (MPa)	Von Mises stress without considering shear stress (Mpa)	Percent
0	Restricted-free	$r=0.1$	346.81	346.58	0.0653%
	Restricted-directed	$r=0.6$	138.901	138.900	0.000097%
0.2	Restricted-free	$r=0.1$	266.94	266.80	0.0531%
	Restricted-directed	$r=0.6$	141.2774	141.2773	0.000102%
0.5	Restricted-free	$r=0.1$	179.82	179.75	0.0395%
	Restricted-directed	$r=0.6$	144.496	144.495	0.000112%
0.8	Restricted-free	$r=0.359$	155.464	155.463	0.00072%
	Restricted-directed	$r=0.1$	147.3032	147.303	0.000124%
1	Restricted-free	$r=0.386$	143.9118	143.9111	0.00054%
	Restricted-directed	$r=0.6$	148.957	148.956	0.000133%

Table 5. Results for elastic limit angular velocity and acceleration for different values of thickness parameter n and $\lambda = -0.5$

Thickness parameter (n)	Boundary condition	Time t (s)	Elastic angular velocity and acceleration	
			Elastic angular velocity ω_e (rad/s)	Elastic angular acceleration $\dot{\omega}_e$ (rad/s ²)
0	Restricted-free	2.36	327	163
	Restricted-directed	3.29	518	259
0.2	Restricted-free	2.61	368	184
	Restricted-directed	3.28	515	257
0.5	Restricted-free	3.05	448	224
	Restricted-directed	3.25	507	253
0.8	Restricted-free	3.10	471	235
	Restricted-directed	3.23	502	251
1	Restricted-free	3.24	505	252
	Restricted-directed	3.16	485	242

7.2.4. Example 4

The effect of thickness parameter n and boundary conditions on of elastic limit angular velocity and acceleration values is investigated in this example. Tables 5-7 lists the values of angular velocity and acceleration in the elastic limit state for various values of constant λ to achieve this goal. At the time t in these tables, the maximum of von Mises equivalent stress in the rotating disk exceeds the disk material's yield strength σ_0 . As seen in these tables, the time at which the disks are yielded is increased by decreasing the constant λ in both boundary conditions. In addition, the influence of constant λ on the values of elastic limit angular acceleration is greater than the influence of its values on the elastic limit angular velocity. In radially restricted-free condition the values of elastic limit angular velocity and acceleration increase by increasing the thickness parameter n . But, as this parameter increases, the values of elastic limit angular velocity and acceleration decreases for the radially restricted-directed conditions. According to Figs. 8 and 9, in this boundary condition, the maximum value of von Mises stress occurs on the outer surface of the disk and disk with a higher thickness parameter has a more equivalent von Mises stress. In terms of boundary conditions, the disk with the radially restricted-directed conditions has more elastic limit angular velocity and acceleration in comparison to the disk with the radially restricted-free conditions.



Table 6. Results for elastic limit angular velocity and acceleration for different values of thickness parameter n and $\lambda = -0.35$.

Thickness parameter (n)	Boundary condition	Time t (s)	Elastic angular velocity ω_e (rad/s)	Elastic angular acceleration $\dot{\omega}_e$ (rad/s ²)
0	Restricted-free	3.35	323	113
	Restricted-directed	4.71	519	181
0.2	Restricted-free	3.75	371	130
	Restricted-directed	4.65	509	178
0.5	Restricted-free	4.30	450	157
	Restricted-directed	4.57	495	173
0.8	Restricted-free	4.50	483	169
	Restricted-directed	4.55	491	172
1	Restricted-free	4.62	503	176
	Restricted-directed	4.53	488	170

Table 7. Results for elastic limit angular velocity and acceleration for different value of thickness parameter n and $\lambda = -0.2$

Thickness parameter (n)	Boundary condition	Time t (s)	Elastic angular velocity ω_e (rad/s)	Elastic angular acceleration $\dot{\omega}_e$ (rad/s ²)
0	Restricted-free	5.86	322	64
	Restricted-directed	8.20	515	103
0.2	Restricted-free	6.70	381	76
	Restricted-directed	8.12	507	101
0.5	Restricted-free	7.55	452	90
	Restricted-directed	8.05	500	100
0.8	Restricted-free	7.90	485	97
	Restricted-directed	8.00	495	99
1	Restricted-free	8.05	500	100
	Restricted-directed	7.90	485	97

8. Conclusions

In this work, the homotopy perturbation method as an analytical solution and finite difference method as a numerical solution were used for the elastic analysis of a rotating annular disk with non-uniform thickness and density under the time-dependent mechanical loading. HPM was successfully employed to obtain the solutions of the equilibrium equation of rotating disk in both radial and tangential directions simultaneously. The obtained results were compared with the FDM solution. In both uniform and non-uniform cases, very good agreement was found. It was shown that the proposed analytical model yields accurate results without the need to use finite element analysis software which is commercially available. This may lead to time and cost-saving in handling complicated cases. The present study also revealed that HPM is a powerful method to be applied to advanced studies of such structures. After validation, numerical examples of HPM results were performed to study the elastic limit angular velocity and acceleration with consideration tangential displacement and shear stress of rotating disks under various thickness parameter n , boundary conditions and constants in angular velocity and acceleration function. The results showed that shear stress has more influence on the distribution of equivalent von Mises stress in the elastic region. The time in which plastic deformation introduced can be improved by considering the smaller value for constant λ . In addition, the type of boundary conditions also affected the distribution of equivalent von Mises stress. It can be concluded that the proposed analytical model can successfully handle the rotating disk problem in general form under mechanical loading and could be expanded to examine more complicated problems of combined loading cases such as thermo-mechanical loadings of gears, turbine rotors, flywheels and other mechanical components.

Author Contributions

Not applicable.

Acknowledgments

Not applicable.

Conflict of Interest

The author declared no potential conflicts of interest with respect to the research, authorship and publication of this article.

Funding

The author received no financial support for the research, authorship and publication of this article.

Data Availability Statements

The datasets generated and/or analyzed during the current study are available from the corresponding author on reasonable request.

Reference

- [1] Gamer, U., Elastic-plastic deformation of the rotating solid disk, *Engineering-Arch*, 54, 1984, 345–354.
- [2] Guven, U., Elastic-plastic stresses in a rotating annular disk of variable thickness and variable density, *International Journal of Mechanical Science*, 43 (2), 1992, 1137–53.
- [3] Guven, U., On the applicability of Tresca's yield condition to the linear hardening rotating solid disk of variable thickness, *Zeitschrift für Angewandte*



Mathematik und Mechanik, 75, 1995, 397–398.

[4] Guven, U., The fully plastic rotating disk of variable thickness, *Zeitschrift für Angewandte Mathematik und Mechanik*, 74, 1994, 61–65.

[5] Eraslan A.N., Orcan, Y., Elastic–plastic deformation of a rotating solid disk of exponentially varying thickness, *Mechanical Material*, 34 (7), 2002, 423–432.

[6] Eraslan A.N., Orcan, Y., On the rotating elastic–plastic solid disks of variable thickness having concave profiles, *International Journal of Mechanical Science*, 44 (7), 2002, 1445–1466.

[7] Eraslan, A.N., Inelastic deformations of rotating variable thickness solid disks by Tresca's and von Mises criteria, *International Journal of Computational Engineering Science*, 3 (1), 2002, 89–101.

[8] Eraslan A.N., Orcan, Y., Von Mises yield criterion and nonlinearly hardening variable thickness rotating annular disks with rigid inclusion, *Mechanical Research Communication*, 29 (5), 2002, 339–350.

[9] Eraslan A. N., Orcan, Y., Elastic–plastic deformations of rotating variable thickness annular disks with free, pressurized and radially restricted boundary conditions, *International Journal of Mechanical Science*, 45 (4), 2003, 643–667.

[10] Hojjati, M.H., Jafari, S., Variational iteration solution of elastic non uniform thickness and density rotating disks, *Far East Journal of Applied Mathematical*, 29, 2007, 185–200.

[11] Hojjati, M.H., Hassani, A., Theoretical and numerical analyses of rotating discs of non-uniform thickness and density, *International Journal of Pressure Vessels and Piping*, 85 (10), 2008, 694–700.

[12] Hojjati, M.H., Jafari, S., Semi exact solution of elastic non uniform thickness and density rotating disks by homotopy perturbation and Adomian's decomposition methods Part I: Elastic Solution, *International Journal of Pressure Vessels and Piping*, 85 (12), 2008, 871–878.

[13] Hojjati, M.H., Jafari, S., Semi-exact solution of non-uniform thickness and density rotating disks. Part II: Elastic strain hardening solution, *International Journal of Pressure Vessels and Piping*, 86 (5), 2009, 307–318.

[14] Hassani, A., Hojjati, M.H., Mahdavi, E., Alashti, R.A., Farrahi, G., Thermo-mechanical analysis of rotating disks with non-uniform thickness and material properties, *International Journal of Pressure Vessels and Piping*, 98, 2012, 95–101.

[15] Jafari, S., Hojjati, M.H., Fathi, A., Classical and modern optimization methods in minimum weight design of elastic rotating disk with variable thickness and density, *International Journal of Pressure Vessels and Piping*, 92, 2012, 41–47.

[16] Alashti, R.A., Jafari, S., The Effect of Ductile Damage on Plastic Behavior of a Rotating Disk with Variable Thickness Subjected to Mechanical Loading, *Scientia Iranica B*, 23 (1), 2016, 174–193.

[17] Zheng, Y., Bahaloo, H., Mousanezhad, D., Mahdi, E., Vaziri, A., Nayeb-Hashemi, H., Stress analysis in functionally graded rotating disks with non-uniform thickness and variable angular velocity, *International Journal of Mechanical Sciences*, 119, 2016, 283–293.

[18] Dai, T., Dai, H.L., Thermo-elastic analysis of a functionally graded rotating hollow circular disk with variable thickness and angular speed, *Applied Mathematical Modelling*, 40 (17–18), 2016, 7689–7707.

[19] Shlyannikov, V.N., Ishtyryakov, I.S., Crack growth rate and lifetime prediction for aviation gas turbine engine compressor disk based on nonlinear fracture mechanics parameters, *Theoretical and Applied Fracture Mechanics*, 103, 2019, 102313.

[20] Nayak, P., Bhowmick, S., Nath Saha, K., Elasto-plastic analysis of thermo-mechanically loaded functionally graded disks by an iterative variational method, *Engineering Science and Technology, an International Journal*, 23 (1), 2020, 42–64.

[21] Bayat, M., Alarifi, I.M., Khalili, A.A., El-Bagory, T., Nguyen, H.M., Asadi, A., thermo-mechanical contact problems and elastic behavior of single and double sides functionally graded brake disks with temperature-dependent material properties, *Scientific Reports*, 9, 2019, 1–16.

[22] He, J.H., Homotopy perturbation technique, *Computational Methods Applied Mechanical Engineering*, 178, (3–4), 1999, 257–262.

[23] He, J.H., Homotopy perturbation method: a new nonlinear analytical technique, *Applied Mathematics and Computation*, 135 (1), 2003, 73–79.

[24] He, J.H., Asymptotology by homotopy perturbation method, *Applied Mathematical Computation*, 6 (3), 2004, 591–596.

[25] He, J.H., Limit cycle and bifurcation of nonlinear problems, *Chaos, Solitons & Fractals*, 26 (3), 2005, 827–833.


[26] He, J. H., Homotopy perturbation method for bifurcation of nonlinear problems, *International Journal of Nonlinear Science and Numerical Simulation*, 6 (2), 2005, 207–8.

[27] Nakamura, S., *Applied Numerical Methods with Software*, Prentice-Hall International Inc, 1991.

[28] Ashok, L., Singh, K., Bhadauria, B.S., Finite Difference Formulae for Unequal Sub-Intervals Using Lagrange's Interpolation Formula, *International Journal of Mathematical Analysis*, 3 (17), 2009, 815 – 827.

[29] Tang, S., Note on acceleration stress in a rotating disk, *International Journal of Mechanical Science*, 12 (2), 1970, 205–207.

ORCID iD

Sanaz Jafari  <https://orcid.org/0000-0001-7574-8169>



© 2022 Shahid Chamran University of Ahvaz, Ahvaz, Iran. This article is an open access article distributed under the terms and conditions of the Creative Commons Attribution-Non Commercial 4.0 International (CC BY-NC 4.0 license) (<http://creativecommons.org/licenses/by-nc/4.0/>).

How to cite this article: Jafari S. Elastic Limit Angular Velocity and Acceleration Investigation in Non-Uniform Rotating Disk under Time-Dependent Mechanical Loading, *J. Appl. Comput. Mech.*, 8(3), 2022, 791–808.
<https://doi.org/10.22055/JACM.2020.32914.2099>

Publisher's Note Shahid Chamran University of Ahvaz remains neutral with regard to jurisdictional claims in published maps and institutional affiliations.

